Phase Delay versus Phase Rotation Cells for Circular Polarization Transmit-Arrays – Application to Satellite Ka-Band Beam Steering

Parinaz Naseri, *Student Member,* Sérgio A. Matos, *IEEE Member,* Jorge R. Costa, *IEEE Senior Member,* Carlos A. Fernandes, *IEEE Senior Member*

Abstract—**Planar transmit-arrays (TAs) have been an attractive solution as gain-enhancers for various applications, e.g. satellite communications. The TA performance directly depends on its composing unit-cells characteristics. Planar unit-cells can be categorized in two main types: phase rotation (PR) and phase delay (PD) cells. There is no hint in the literature about the relative merits of these two types of cells for circular polarization when assessing the final TA performance. This paper offers a systematic comparison between the cells' working principles and analyses their impacts on a TA performance. An example of a PR-based TA and a PD-based TA are designed for single-band wide-angle beam steering operating at the Satellite Ka-band. They are evaluated by simulation and measurement to quantify performance differences. No previous work employed a PR-TA for wide-angle beam steering. This work shows that PR-TA offers a filtering effect toward the cross-polarization component of the source. This leads to better axial ratio and combined 3 dB axial ratio and 3 dB gain bandwidth. However, PD cells are easier to design and insensitive to the feed polarization. The analysis in the paper allows a more informed decision when selecting the unit cell category for any given TA application.**

***Index Terms*—flat lens, transmit-arrays, mechanical scanning, frequency selective surface (FSS), circular polarization, wireless communication network, satellite-on-the-move (SOTM).**

I. Introduction

TRANSMIT-ARRAYS (TA) have been an attractive solution to achieve high-gain pencil-beam in many applications such as point-to-point links and satellite communications due to their potential low-weight, moderate-profile, low-cost, high efficiency, simple feed network, and no feed blockage effect [1]. The working principle of a TA is similar to the one of a dielectric lens [2] in which each zone of the lens or TA adds an appropriate phase shift to the field passing through it. While in a lens, this is met by adjusting the lens profile, in a TA, this is achieved by adjusting each phase shift provided by individual unit-cells with constant thickness populating the TA. Therefore, comparing to a lens with the same gain, a TA has much less mass and offers more flexibility to use the available horizontal space for beam scanning.

The unit-cells should have minimum reflection and minimum insertion loss, while ensuring a phase shift range up to 360˚ in order to correct the phase of the incident wave at each point of the TA surface. The amount of phase shift required for a cell is dependent on the desired phase of the outgoing wave at cell position of the TA minus the phase shift that the incident wave endures from the feed until it reaches that cell position.

There are several different types of TA unit-cells. For example, they can be implemented by connecting the two parallel sides of the TA through variable length of transmission lines [3], by coupling the TA surfaces through various shapes of inclusions [4], [5], [6], by stacking sub-wavelength capacitive patches and inductive grids [7], or by using artificial engineered materials [8]-[9]. Among the aforementioned types of cells, the elements composed of planar patches and/or slots have low losses and low thickness, and they are easy to fabricate using printed circuit board (PCB) technology. Therefore, this kind of cells has been extensively employed in both fully passive and reconfigurable structures.

In some satellite communications, the ground terminal might be on the move. Thus, in order to maintain the link between the two communication ends, beam steering capability is required at the ground terminal antenna. Beam steering in TAs can be obtained by electrically tuning the phase shift [14]-[15] of reconfigurable cells or mechanically moving the primary feed or the TA [16]-[18]or a hybrid solution [19]. The first approach offers fast beam-steering, with no wearable parts. However, reconfigurable TAs suffer from low phase resolution, high losses, and low reliability of some of the available options at high frequencies as for the satellite communications Ka-band (20-30 GHz) [20]. Consequently, printed passive patch based-TAs with mechanical beam-steering capability are currently more promising for satcom at Ka-band.

Circular polarization (CP) has been a key consideration in the design of TAs for any communication link in which the misalignment of the transmit and receive antennas or Faraday's effect might introduce loss or error [21]. A CP high-gain beam

Manuscript received August, 2017. This work is partially supported by the Fundação para a Ciência e a Tecnologia under the grant UID/EEA/50008/2013.
Parinaz Naseri, Sérgio A. Matos, Jorge R. Costa, and Carlos A. Fernandes are with Instituto de Telecomunicações, Instituto Superior Técnico, Universidade de Lisboa, Av. Rovisco Pais 1, 1049-001 Lisboa, Portugal (phone +351-218418480 fax +351-218418472 e-mail parinaz.naseri@lx.it.pt).

Sérgio A. Matos and Jorge R. Costa are also with Instituto Universitário de Lisboa (ISCTE-IUL), Departamento de Ciências e Tecnologias da Informação Av. das Forças Armadas, 1649-026 Lisboa, Portugal.

can be obtained by illuminating a TA of double linearly polarized (LP) unit-cells by a CP feed [16] or by feeding a TA of sequentially rotated CP unit-cells with an LP feed [22] or a CP source [4], [23].

This work focuses on TAs with passive patch cells for CP beam steering applications, fed by a CP source. There are generally two approaches to generate different phase shifts from a designed passive unit-cell. These approaches include varying the center frequency of the designed unit-cell [7], [16], and rotating the designed unit-cell [4], [22], [23]. The first approach leads to designing a discrete number of cells with slightly different geometries, all with good transmission coefficients within a certain frequency band, but providing different phase shifts at that band. We call this type the "phase delay (PD)" cells throughout this paper. The second approach is where only one unit-cell is designed and then rotated with different angles to provide a continuous phase shift up to 360°. We name these the "phase rotation (PR)" cells.

We believe that the detailed knowledge about the unit-cells' impact on the TA performance can contribute to achieving the best performance with the available resources. Therefore, in this paper, we compare the two categories of passive patch elements and thoroughly explain their physical and electrical differences, and their effects on the TA system performance. While the literature on the topic lacks such information, this work presents a detailed comparison of the advantages and disadvantages of the two unit-cell categories. To better illustrate these points, an example of PD and PR cells is presented and used to generate two corresponding TAs. These are designed to achieve high-gain circularly polarized pencil-beam with wide-angle beam steering capability for satellite communications at Ka-band.

This paper is organized as follows. In Section II, the working principles of the PD and PR cells for circular polarization are explained. Section III presents an example of each PD and PR cell and provides thorough analysis of the performance of each cell. In Section IV, the full-wave simulation results of two gain-enhancing TAs composed of the introduced PD and PR cells are presented. The compared performance of each TA and its verification by measurement results is presented in Section V.

II. Operation Principle of Phase Delay and Phase Rotation Cells

A. Working principle of the cells

Unit-cell scattering parameters (S-parameters) can be defined in right (r) and left (l) circular polarizations (CP). These parameters are dependent on the orthogonal x- and y-linear polarization (LP) scattering parameters [4]. Here, we define two coordinate systems, one for the TA and another for each individual cell (see Fig. 1). While the first has fixed axes (x, y, z), the in-plane axes of the later (x', y', z) change based on the cell rotation. These coordinate systems are depicted in Fig. 1. The CP S-parameters of any kind of rotated unit-cell that is symmetric in relation to the z axis, are summarized below using the same nomenclature as in [4]:

$$\begin{bmatrix} b_{1l} \\ b_{1r} \\ b_{2l} \\ b_{2r} \end{bmatrix} = \begin{bmatrix} \Gamma_{ll} & \Gamma_{lr} & T_{ll} & T_{lr} \\ \Gamma_{rl} & \Gamma_{rr} & T_{rl} & T_{rr} \\ T_{ll} & T_{lr} & \Gamma_{ll} & \Gamma_{lr} \\ T_{rl} & T_{rr} & \Gamma_{rl} & \Gamma_{rr} \end{bmatrix} \begin{bmatrix} a_{1l} \\ a_{1r} \\ a_{2l} \\ a_{2r} \end{bmatrix}, \quad (1)$$

where the reflection and transmission coefficients are:

$$\Gamma_{ll} = 0.5(\Gamma_{x'x'} - \Gamma_{y'y'} + j\Gamma_{x'y'} + j\Gamma_{y'x'})e^{-j2\psi} \quad (2)$$

$$\Gamma_{rr} = 0.5(\Gamma_{x'x'} - \Gamma_{y'y'} - j\Gamma_{x'y'} - j\Gamma_{y'x'})e^{+j2\psi} \quad (3)$$

$$\Gamma_{rl} = 0.5(\Gamma_{x'x'} + \Gamma_{y'y'} + j\Gamma_{x'y'} - j\Gamma_{y'x'}) \quad (4)$$

$$\Gamma_{lr} = 0.5(\Gamma_{x'x'} + \Gamma_{y'y'} - j\Gamma_{x'y'} + j\Gamma_{y'x'}) \quad (5)$$

$$T_{rr} = 0.5(T_{x'x'} + T_{y'y'} - jT_{x'y'} + jT_{y'x'}) \quad (6)$$

$$T_{ll} = 0.5(T_{x'x'} + T_{y'y'} + jT_{x'y'} - jT_{y'x'}) \quad (7)$$

$$T_{lr} = 0.5(T_{x'x'} - T_{y'y'} - jT_{x'y'} - jT_{y'x'})e^{+j2\psi} \quad (8)$$

$$T_{rl} = 0.5(T_{x'x'} - T_{y'y'} + jT_{x'y'} + jT_{y'x'})e^{-j2\psi}, \quad (9)$$

and ψ is the rotation angle between the TA (x, y, z) coordinate system and the unit-cell (x', y', z) coordinate system, see Fig. 1.

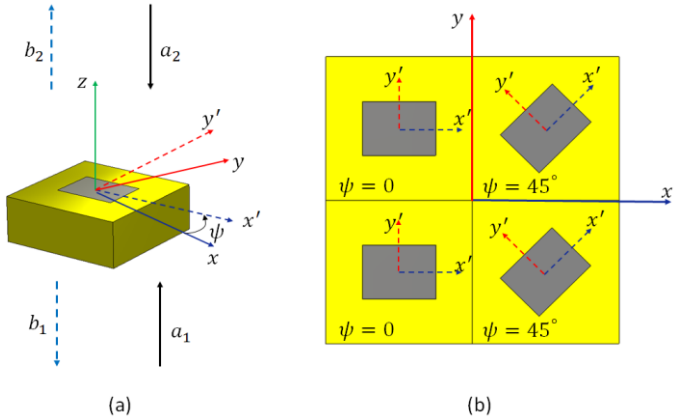

Fig. 1 Coordinate system of the transmit-array (x, y, z) and coordinate system of the unit-cell (x', y', z): (a) unit-cell; (b) transmit-array.

PD and PR unit cells have distinct operation functions based on different working principles beside their geometric differences. In a set of PD cells, the range of $0° - 360°$ phase shift is obtained by adjusting the dimensions of the composing metallic elements comparing to a reference cell. Therefore, in a collection of PD cells that include N distinct unit-cells, N discrete phase shifts are accessible. In fact, each discrete phase shift is associated with a specific PD cell that has its specific transmission and reflection coefficients. It can become challenging to design a PD cell with specific phase shift with high transmission. This double requirement for each PD cell in the set can become increasingly complex when high resolution and high number of different PD cells are required. As a result, a set of PD cells include cells that some of which offer lower transmission coefficients but distinct phase shift.

The general equations (2) – (9) can be specifically written for a set of PD cells. In this paper we will refer only to PD cells for circular polarization operation. In this case a PD cell must present the same performance for x' and y' linear polarizations. Therefore, the cell must be double symmetric regarding x' and y' axes and its shape shall not change if rotated by 90º. Moreover, since none of the N PD cells are rotated, the

coordinate system of each cell matches the coordinate system of the TA (i.e. $\psi = 0$; $x = x'$; $y = y'$). Therefore, for the n-order PD cell ($1 \le n \le N$):

$$\psi = 0 \tag{10}$$
$$T_{xx}^n = T_{yy}^n = |T^n| e^{j\Delta\varphi_n} \tag{11}$$
$$T_{xy}^n = T_{xy}^n = 0 \tag{12}$$
$$\Gamma_{xx}^n = \Gamma_{yy}^n = |\Gamma^n| e^{j\Delta\varphi_n} \tag{13}$$
$$\Gamma_{xy}^n = \Gamma_{xy}^n = 0, \tag{14}$$

where $\Delta\varphi_n$ is the relative phase shift provided by the n-order unit-cell in the PD collection. This relative phase shift is the same for the transmission and reflection coefficients because it is assumed that the cell is symmetric in relation to the z axes. Thusly, by replacing in (2)-(9),

$$T_{rr\_PD}^n = T_{ll\_PD}^n = 0.5\left(T_{xx}^n + T_{yy}^n\right) = |T^n| e^{j\Delta\varphi_n} \tag{15}$$
$$T_{lr\_PD}^n = T_{rl\_PD}^n = 0.5\left(T_{xx}^n - T_{yy}^n\right) \cong 0\, e^{j\Delta\varphi_n} \tag{16}$$
$$\Gamma_{lr\_PD}^n = \Gamma_{rl\_PD}^n = 0.5\left(\Gamma_{xx}^n + \Gamma_{yy}^n\right) = |\Gamma^n| e^{j\Delta\varphi_n} \tag{17}$$
$$\Gamma_{rr\_PD}^n = \Gamma_{ll\_PD}^n = 0.5\left(\Gamma_{xx}^n - \Gamma_{yy}^n\right) \cong 0\, e^{j\Delta\varphi_n}. \tag{18}$$

Coefficients $T_{lr\_PD}^n$ and $\Gamma_{rr\_PD}^n$ are assumed to be close to zero and not exactly zero because, when the cell is integrated in a TA, its neighboring cells are no longer identical. Thus, the conventional periodic boundary assumption used for the unit-cell design to obtain the cell S-matrix is no longer valid.

On the contrary, the phase shift in PR cells is achieved by rotating the cell around its perpendicular axes. In fact, for each value of the phase shift, the geometry of the PR cell is unchanged, only rotated by a certain $\psi°$ angle. Therefore, PR cells lead to a continuous range of phase shifts between 0° and 360° with almost constant amplitude of the transmission and reflection coefficients.

PR cells must behave distinctively for the two orthogonal linear components of an incident wave, such that they transmit both components with equal magnitude and 180° phase difference [23]. This requirement dictates that an ideal PR cell be double symmetric regarding x' and y' axes, but its orientation changes regarding the previous axes once it is rotated by 90º. Any discrepancy from this case leads to degradation of CP transmission coefficient and increase in the CP cross component level once the cell is rotated. For example, the proposed PR cell in [22] experiences a great amount of increase in cross-polarization amplitude once it is rotated by 90° or 180°. Furthermore, due to these requirements for transmission coefficients, the resultant geometry provides also linear reflection coefficients with almost equal amplitude and 180° phase difference. Therefore, for the PR cell:

$$T_{x'x'} = -T_{y'y'} = T \tag{19}$$
$$\Gamma_{x'x'} = -\Gamma_{y'y'} = \Gamma \tag{20}$$
$$T_{x'y'} = T_{y'x'} = \Gamma_{x'y'} = \Gamma_{y'x'} = 0, \tag{21}$$

and by replacing in (2)– (9)

$$T_{rr\_PR}^{\psi} = T_{ll\_PR}^{\psi} = 0.5\left(T_{x'x'} + T_{y'y'}\right) \cong 0 \tag{22}$$
$$T_{lr\_PR}^{\psi} = 0.5\left(T_{x'x'} - T_{y'y'}\right) e^{+j2\psi} = T e^{+j2\psi} \tag{23}$$
$$T_{rl\_PR}^{\psi} = 0.5\left(T_{x'x'} - T_{y'y'}\right) e^{-j2\psi} = T e^{-j2\psi} \tag{24}$$
$$\Gamma_{lr\_PR}^{\psi} = \Gamma_{rl\_PR}^{\psi} = 0.5\left(\Gamma_{x'x'} + \Gamma_{y'y'}\right) \cong 0 \tag{25}$$
$$\Gamma_{rr\_PR}^{\psi} = 0.5\left(\Gamma_{x'x'} - \Gamma_{y'y'}\right) e^{+j2\psi} = \Gamma e^{+j2\psi} \tag{26}$$
$$\Gamma_{ll\_PR}^{\psi} = 0.5\left(\Gamma_{x'x'} - \Gamma_{y'y'}\right) e^{-j2\psi} = \Gamma e^{-j2\psi}, \tag{27}$$

the phase shift provided by the PR unit-cell is presented with $2\psi°$ when the cell is rotated by $\psi°$. Again, the close to zero value instead of null coefficients is justified by the slightly different response that the cell presents when integrated in an actual TA with neighboring cells with different rotation values.

B. PD versus PR beam collimating transmit-arrays

Based on the general properties of PR and PC cells identified in the previous section, it is possible to anticipate distinct general behaviors of TAs formed by the two types of cells, irrespective of their practical realization. In the family of PD cells, coefficients $T_{lr\_PD}^n$ and $\Gamma_{rr\_PD}^n$, in equations (16) and (18) respectively, are very close to zero. As a result, the main transmitted CP wave from a PD-TA has the same polarization as the incident wave, while the main reflected CP wave has the opposite sense. Moreover, not only does a PD-cell provide phase shift in the main transmitted co-polarized wave, it also applies phase shift to the cross-polarized transmitted wave and the reflected waves. Hence, when a PD-TA is designed to collimate the feed radiation towards a specific direction $\alpha_0°$, the cross polarized transmitted wave also gets focused in the same direction while the reflected back-lobe is collimated in the direction of $(180 - \alpha_0)°$, see Fig. 2 (a).

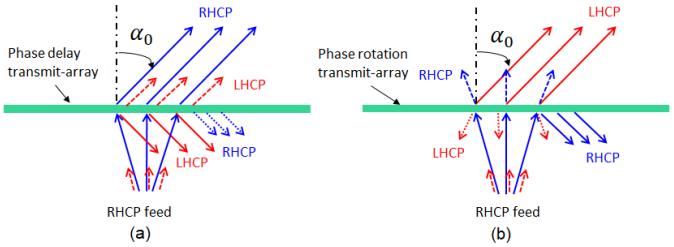

Fig. 2 Illustration of how (a) phase delay and (b) phase rotation TAs work. The length of the arrows represents the approximate comparison between the intensity of all the CP beams within the same cell type. All the red lines present LHCP radiation and all the blue line present RHCP radiation.

It is worth mentioning that the aforementioned cross-polarization can have three origins: S-parameters of each unit-cell, the distribution of the cells in a TA, and/or the impurity of the CP from the feed antenna. In a PD-TA, this cross-polarization does not stem from the S-parameters of the PD cells since $T_{lr\_PD}^n$ and $T_{rl\_PD}^n$ are almost zero for all of the PD cells even for up to 30° oblique incidence. However, if the distribution of these cells in a PD-TA is asymmetric, a cross-polarization component is generated. Furthermore, the cross-polarization can be more importantly caused by the impurity of the CP radiation from the feed antenna. The sense of the CP incidence is indifferent to the PD cells and they provide the same phase shift to a RHCP incidence or LHCP one. In other words, $T_{rr\_PD}^n$ is equal to $T_{ll\_PD}^n$ for a PD unit-cell. Therefore, the cross polarization from the feed also gets focused in the same direction of the main co-polarized beam.

In the PR cells, $T_{rr\_PR}^{\psi}$ and $\Gamma_{lr\_PR}^{\psi}$ in equations (22) and (25) are close to zero. This is achieved due to the symmetric linear

transmission coefficients ($T_{y'y'\_PR} = -T_{x'x'\_PR}$) and symmetric linear reflection coefficients ($\Gamma_{y'y'\_PR} = -\Gamma_{x'x'\_PR}$). However, it is difficult to minimize $T^{\psi}_{rr\_PR}$ transmission for a wide frequency band. Basically, to design a wideband PR cell, the phase of the x'- and y´-polarization transmission coefficients must present the same slope vs frequency and 180º difference between them, while the amplitude must remain constant over that band. Since this requirement is hard to be translated to the physical geometry of a cell, the PR cells tend to have a narrower band-width compared to the PD cells.

To explain the working principle, consider as an example that the incident wave in the TA is RHCP. All statements are conversely true for an LHCP incident wave. For RHCP incidence, the TA transmits the major part as a collimated LHCP wave, while applying a phase shift to it. Nonetheless, in a real designed PR-TA, a small part of the RHCP incident wave goes through the PR cell as RHCP wave with no phase shift. Consequently, the cross polarization generated by the cell never gets collimated or redirected to any specific direction.

Moreover, a PR-TA behaves differently with respect to the impurity of the CP radiation from the feed antenna compared to the PD-TA. Unlike a PD unit-cell, according to equations (23) and (24), a rotated PR cell applies different phase shifts to RHCP or LHCP incident waves. For example, let us consider a PR cell that is rotated clockwise by ψ°. If this cell gets illuminated by an RHCP wave, the major transmission to the other side of the cell is an LHCP wave with $2\psi^{\circ}$ phase shift comparing to the incidence. However, if the same cell gets illuminated by an LHCP wave, the transmitted wave is an RHCP wave with $-2\psi^{\circ}$ phase shift. Therefore, firstly, the polarization of the feed antenna is important in the design of the PR-TA (a TA designed for RHCP incidence will not work for an LHCP source). Secondly, a PR-TA does not focus, but else diverges the cross-polarization component of the feed.

Furthermore, equations (26) and (27) show that the back-lobe radiation at $(180 - \alpha_0)°$ from a PR-TA only stems from the reflected wave with the same CP sense as the feed. While, from equation (25), a non-collimated reflection with the orthogonal polarization of the feed is reflected back to 180º. Fig. 2 summarizes and compares the aforementioned behaviors.

III. Phase Delay and Phase Rotation Unit-Cells

The analysis from the previous section is general for any PR or PD cell configuration. This section compares the performance of a practical example of a PD cell versus a PR cell. The interest is centered on the transmission characteristics across the band for normal and oblique incidence. Both unit-cells are simulated using the commercial software ANSYS HFSS [24] using the frequency domain (FD) solver with local periodic boundary condition (PBC) and Floquet-modes excitation.

A. Phase Delay (PD) cell example

The PD cells in this work are the same used in [16], designed for the uplink frequency of satellite communications in the Ka-band (30 GHz). The cell is composed of 5 subwavelength square capacitive patches with side lengths of L1, L2, and L3. Each cell includes a pair of L1 patches, a pair of L2 patches, and a single L3 patch as shown in Fig. 3. The metallic patches are stacked with four 0.787mm-thick Duroid 5880 dielectric layers with $\varepsilon_r = 2.2$ and $tan\delta = 0.0009$. The in-plane size of the cell is $W_{PD} = 2.5mm$ ($\lambda_0/4$ at 30GHz) and the total thickness of the cell is T_{PD} = 3.35mm.

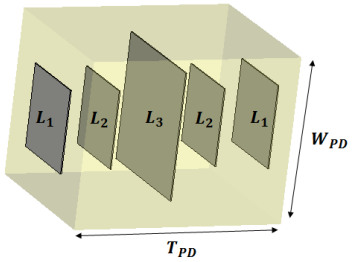

Fig. 3 Phase delay (PD) unit-cell (square patches with side length of L1, L2, and L3) [16].

By varying the dimensions of the patches in a unit-cell it is possible to vary the phase shift of the transmission coefficient from 0 to 316º, see Fig. 4. This range is chosen as an acceptable trade-off between the TA performance and the number of metallic layers. 63 PD cells were designed to cover the above phase shift range with 5.4° steps in average. Based on the study performed in [16], the transmission coefficient of all cells is better than -0.55 dB within the Ka-uplink band (i.e. 29.5 GHz-30 GHz). Also, the reflection coefficients of all PD cells are lower than -9.5dB within the bandwidth under normal incidence. The performance of this PD cell type has been verified experimentally in [16].

As the usual case in the literature, the design of the PD cells is performed assuming normal wave incidence at the cell surface. However, in a large TA, the incidence angle at the unit-cell can increase significantly towards the edges of the TA. Fig. 4 also presents the variation of the phase shift of the PD cell family for oblique incidence angles up to 45º. It is shown that the phase shift range provided by the 63 PD cells decreases from [0º, 316º] to [-12.7º, 250.7º] as the incidence angle increases to 45º. This may lead to phase errors in the aperture of large TAs with the consequent reduction of the measured gain compared to the expected value. The amplitudes of transmission and reflection coefficients of the PD cells also degrade with the increase of the angle of incidence. For some of the 63 cells, the transmission coefficient can reduce to -2.1 dB and the reflection coefficient can increase up to -4.5 dB for 45º- incident angle.

Collimating TAs necessarily require different side-by-side cells with different phase shifts. The largest difference usually occurs at the 360º jump rings. Therefore, the conventional periodic boundaries assumption used to obtain the unit-cell's S-matrix through simulation is not completely valid in TAs. The effect was analyzed for these PD cells in [25].

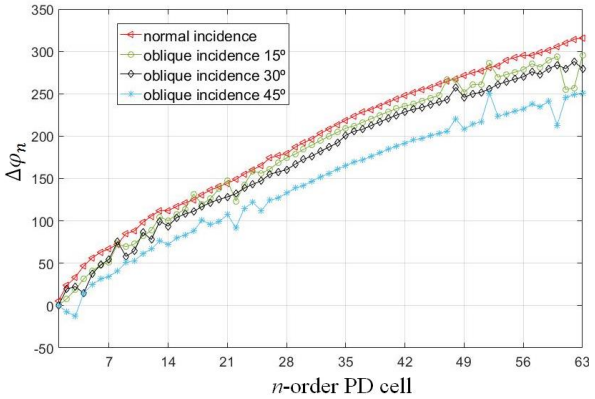

Fig. 4 Transmission phase ($\Delta\varphi_n$) of the PD unit-cells at 30GHz under normal and oblique incidences.

B. *Phase Rotation (PR) cell example*

An anisotropic cell similar to [23] and [26] was designed as an example of a PR cell. It is composed of three metal layers separated by 0.508 mm-thick Duroid 5880 dielectric slabs. The design of the cell is based on antenna-filter-antenna structure described in [26]. The in-plane width of the unit-cell is $W_{PR} = 5\ mm$ ($\lambda_0/2$ at 30 GHz) and the total thickness is T_{PR} = 1.05 mm. Fig. 5 shows the structure of this cell; its dimensions are summarized in Table I. The role of each element is thoroughly explained in [26]. Cell rotation by $\psi°$ about the z-axis introduces a $2\psi°$ phase shift in the transmission coefficient. So the 0 to 360° variation of the phase shift is simply achieved by 0 to 180º rotation of the unit-cell. Therefore, the phase shift provided by a PR cell can be continuous and not discretized as it is in the PD cells.

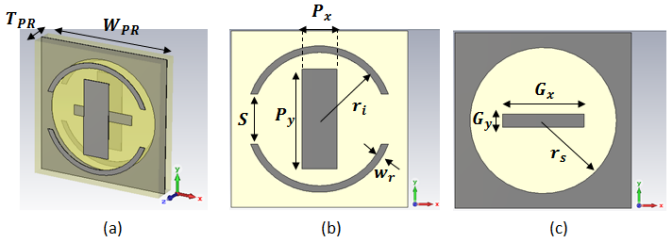

Fig. 5 Phase rotation (PR) unit-cell: (a) 3D view, (b) first layer, and (c) second layer.

TABLE I
DIMENSIONS OF THE PR UNIT CELL

Dimension	Size (mm)	Dimension	Size (mm)
W_{PR}	5	S	1.5
T_{PR}	1.05	w_r	0.2
P_x	1.05	G_x	2.35
P_y	3.05	G_y	0.45
r_i	1.9	r_s	2.1

Fig. 6 shows the frequency response of the transmission and reflection coefficients of a uniform TA formed by these unit-cell (all with ψ=0º rotation), illuminated by an RHCP incident wave. The transmission coefficients of the PR cell, T_{rr_PR} and T_{rl_PR}, were measured by placing a planar surface of identical non-rotated PR cells in the middle of a direct link between two horns. The results have confirmed the expected behaviour of the PR cells, as seen in Fig. 6. Identical curves are obtained for LHCP incident wave. As mentioned before, the unit-cell is designed such that the opposite sense of incident wave circular polarization gets transmitted, while the phase is controllable through the cell rotation. According to Fig. 6, this transmission is better than -0.85 dB within the Ka-uplink band (marked as a grey bar in the figures). The transmitted cross-polarization level is about -10 dB. However, this level is expected to decrease if the unit-cells are used in a focusing TA, since the cross-polarized wave does not get collimated through the TA. This is because the phase of the transmission coefficient in (22) does not change with $\psi°$ rotation. In terms of the reflection coefficient, its value is below -12 dB within the band, a better value than some PD cells [16]. Nevertheless, it is noticeable that the transmission coefficient value of the PR cell, in Fig. 6, drops to lower values out of the operating bandwidth when compared to the PD cells [16] (e.g. for 29 GHz $T^n > -0.8$ dB for all cells, while $T_{rl} = -1.25$ dB).

The reflection and transmission frequency response of the cell for different incident angles is presented in Fig. 7. We can see that in all coefficients the variations are minor for incident angles up to 45°. For example, the transmission loss increases to 1 dB for 45° oblique incidences, see Fig. 7 (c). This somewhat resilience to oblique incident angles is mainly due to the use of a thinner cell comparing to the PD ones.

In a PR-TA, while all of the cells have the same geometry, they are rotated with different ψº angles. That is why, it is important to verify the stability of the PR cell's response for different rotation angles. The key factor is the variation in the coupling between adjacent cells once the cells are rotated. Generally, rotated slot-rings experience less change in the coupling with the similar neighbor cell, compared to rectangular shapes that are much more influenced by this effect. For example, for the presented PR cell, the slot-rings, in the first and the third layers, present similar couplings independent of the relative rotation between adjacent cells. Nonetheless, once the PR cell is rotated, the coupling between the rectangular adjacent elements changes and consequently the response of the unit-cell also alters. Due to the cell geometry, it is verified that the cell response is identical for a rotation of ψ = 0º, 90º and 180º. Fig. 8 shows the dependence of the cell's S-parameters on the rotation angle from ψ = 0º to 45º. Comparing to the initial state, the transmission coefficient decreases 0.1 dB and the transmitted cross polarization increases by 1 dB, while the reflections decrease. In the proposed structure, the size of the S gap in the rings and of the first and the third rectangular elements have the most impact on the amount of coupling. The bigger the rectangle lengths and the smaller the S gap, the more variation in the amplitude of the coefficients occurs with the cell $\psi°$ rotation.

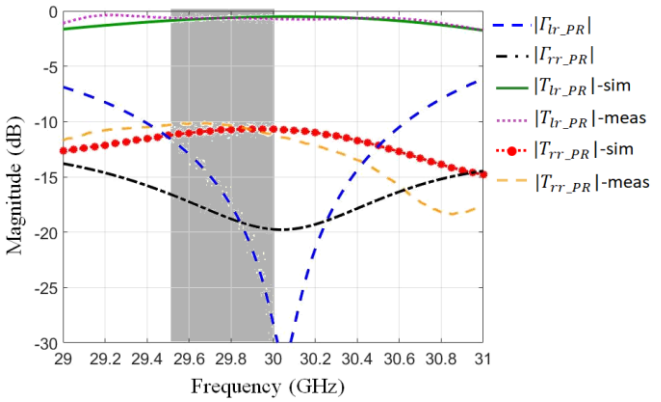

Fig. 6 Circular polarization scattering parameters of the PR cell for normal incidence along with the measured transmission coefficients.

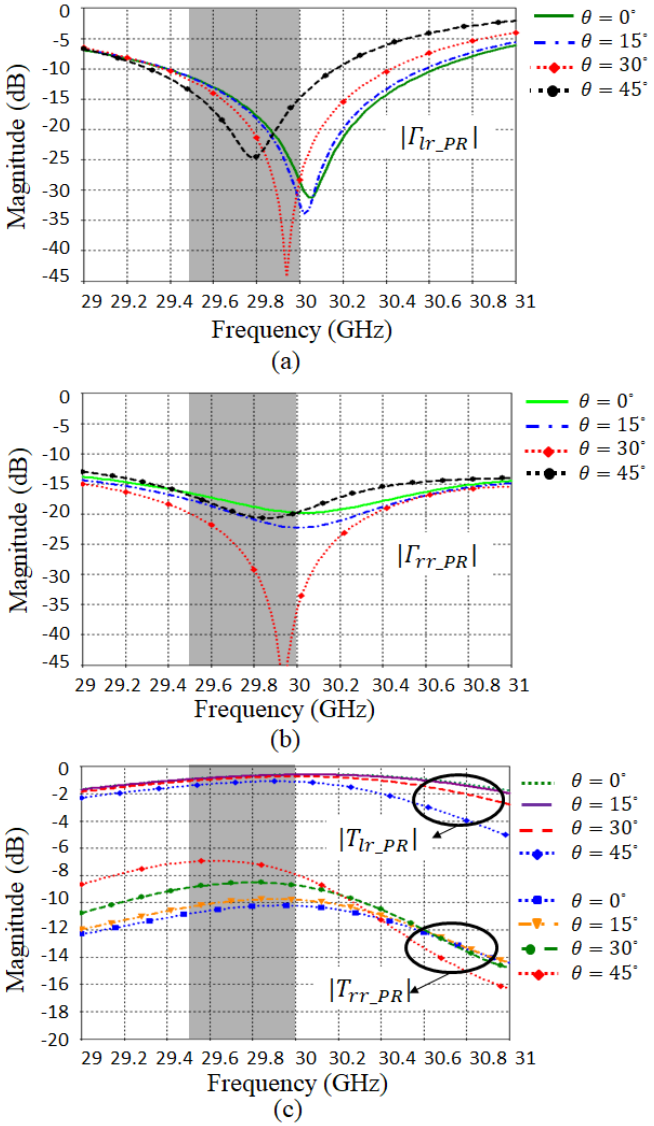

Fig. 7 (a) Reflection coefficient Γ_{lr_PR}; (b) reflection coefficient Γ_{rr_PR} and (c) transmission coefficients T_{lr_PR} and T_{rr_PR} of the PR cell for different incident angles.

Finally, based on simulations of both presented examples of the PD unit-cells and PR-cell, we evaluated the sensitivity of their design to fabrication inaccuracies in terms of over-etching and misalignment between the layers. The analysis confirms that with misalignment up to 500um and maximum over-etching of $50\mu m$, which are the achievable accuracies in our university lab, both PD-cells and PR-cell maintain transmission coefficients better than -1.6dB with maximum phase variation of 25º.

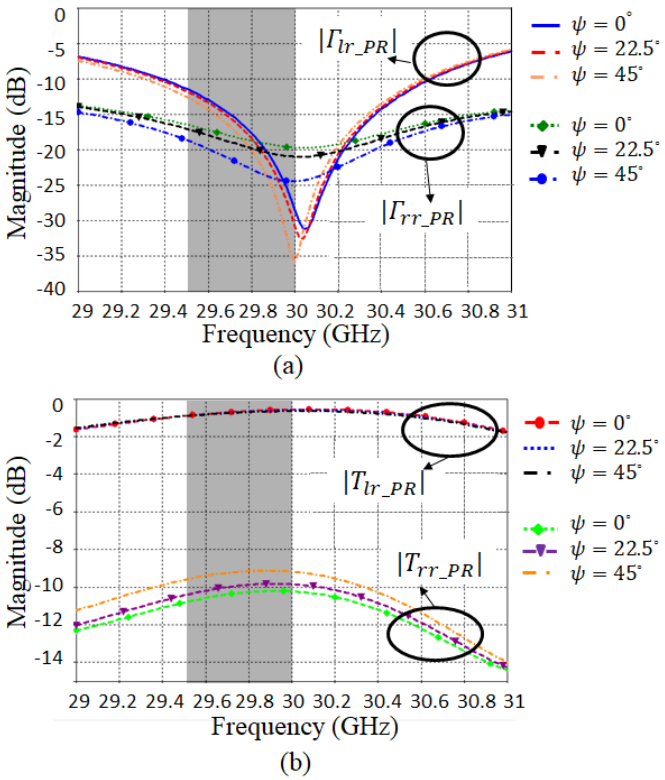

Fig. 8 (a) Reflection and (b) transmission coefficients of the PR cell for different rotation ψ angles under normal incidence.

IV. Examples of Phase Delay and Phase Rotation Transmit-Arrays

In this section, we compare two TAs based on the introduced PD and PR cells. These full-wave simulated TAs are 140 mm × 190 mm and similar to the one fabricated in [16]. One of the TAs is composed of 76 × 56 PD cells (see Fig. 9(a)) while the other is composed of only 38 × 28 PR cells (see Fig. 9 (b)) due to the double size of the designed PR cells when compared to the PD cells. Throughout this paper, we designate the field phase term as φ according to the notation $e^{-j\varphi}$.

The phase correction function of the TAs is calculated based on [16]

$$\varphi_{lens}(x,y) = k_0\left[x\sin(\alpha_0) - \sqrt{x^2+y^2+F^2}\right] \quad (28)$$

where focal distance F is 100 mm and the collimated beam direction is $\alpha_0 = 32.5°$ (with respect to the aperture normal) when the feed is at the focal position. The configurations of the two TAs are shown in Fig. 9 (a) and Fig. 9 (b), respectively, where they are fed by an $x-$polarized horn. The TAs are fed in the simulations by standard gain Ka-band rectangular horn (Flann Microwave N° 122240-15) with 14.1 dBi gain at 30 GHz, successively with two orthogonal linear polarizations. For each TA, the linear polarization results from x− and y−polarized horn are combined based on (29) where E_a^b presents the patterns of the E-field in b−direction (θ or φ) when electric field on the aperture of the horn is a −polarized (x or y) to obtain the circular polarization patterns of each TA to an ideal RHCP wave $((\overrightarrow{E_x} - j\overrightarrow{E_y})/\sqrt{2} = (E_x^\theta\hat{\theta} + E_x^\varphi\hat{\varphi} - jE_y^\theta\hat{\theta} - jE_y^\varphi\hat{\varphi})/\sqrt{2})$ illumination. In this way, it is possible to isolate the TA

polarization behavior from the potential polarization impurity of an alternative circular polarization feed.

$$E_{RHCP} = \frac{E_x^{\theta} + jE_x^{\varphi} - jE_y^{\theta} + E_y^{\varphi}}{2} \quad (29)$$

It is worth mentioning that due to the different rotation angles of the PR cells, their detailed structure, and circular geometry, a solver based on tetrahedral meshing provides much more accurate results than hexahedral meshing based solver, when compared for similar computational resources and time. Both TAs are simulated in ANSYS HFSS [24] using the frequency solver. In order to save memory and computational time, the hybrid finite element-boundary integral (FE-BI) method available by HFSS is employed to avoid unnecessary meshing of the free space volume.

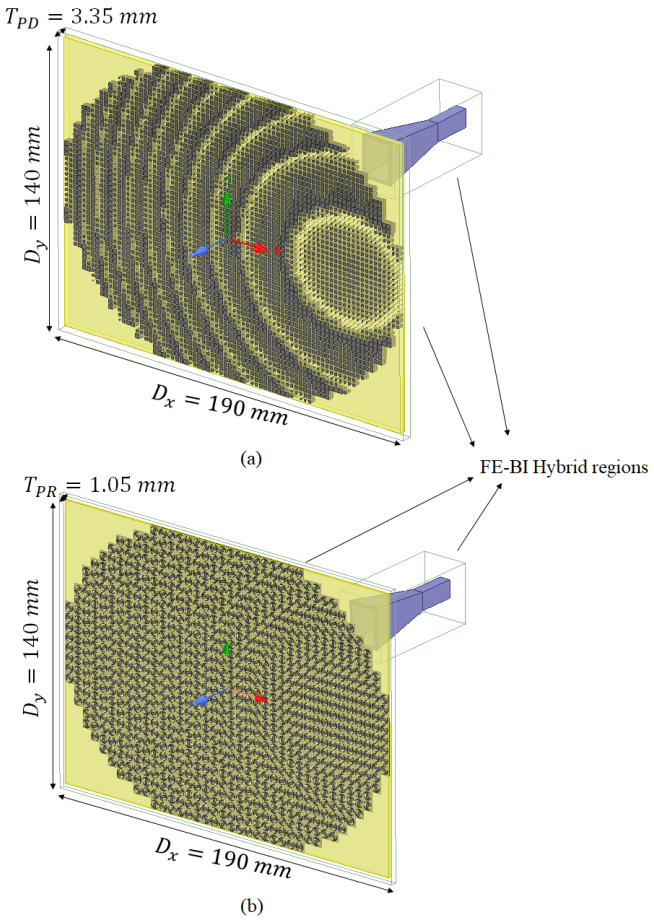

Fig. 9 Configuration of the (a) PD and (b) PR-TAs used for full-wave simulations in Ansys HFSS [24].

A. PD transmit-array simulations

The simulation results of the PD-TA shown in Fig. 9 (a) are presented in Fig. 10 for the feed central position. We can see that the TA successfully focusses the RHCP radiation of the feed antenna to an RHCP pencil beam pointing at 32.5° direction. The directivity of this antenna is 29.6 dBi at 30 GHz. Moreover, as explained before, it is noticeable that the cross-polarization is also focused to $\alpha_0 = 32.5^{\circ}$ due to the phase correction applied by the PD-TA on the cross-polarized transmission coefficient (i.e. $T_{lr\_PD}^{n}$ from (16)). This effect leads to the main beam cross-polarization level of 17.6dB and degrades the axial ratio of the main beam to 2.3 dB. The PD-TA, as explained before, collimates both RHCP and LHCP reflected waves to $180° - \alpha_0 \approx 148°$ due to the phase correction implied in $\Gamma_{lr\_PD}^{n}$ from (17) and $\Gamma_{rr\_PD}^{n}$ from (18). However, these reflections are respectively 24.2 dB and 19.9 dB lower than the gain of the main lobe.

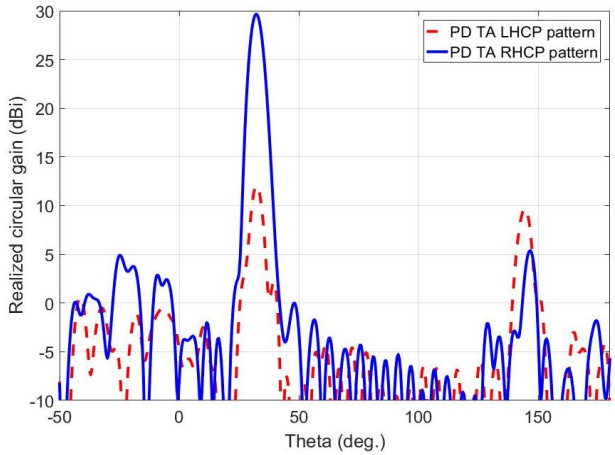

Fig. 10 Simulated performance of phase delay (PD) transmit-array.

B. PR transmit-array simulations

The simulation results of the PR-TA presented in Fig. 9 (b) are shown in Fig. 11. The PR-TA collimates the radiation from an RHCP feed source to an LHCP radiation pointing to α_0=32.5° with the gain of 29.6 dBi at 30 GHz, similar to the gain of the PD-TA. The TA applies no phase shift on the transmitted RHCP waves (i.e. $T_{rr\_PR}^{\psi}$ from (22)). Therefore, unlike the PD-TA, the cross-polarization is not refracted by the TA and follows the feed radiation direction instead of the main beam direction. This is seen in Fig. 11 around $\theta = 0°$. The PR-TA presents a much better main beam axial ratio of 1.02 dB calculated from main beam cross-polarization level that is 24.6 dB. It can also be seen that only the cross-polarization component (i.e. RHCP radiation) is collimated to 148° ($\cong 180° - \alpha_0$) due to the phase correction introduced by the PR-TA on the co-polarized reflection coefficient (i.e. $\Gamma_{rr\_PR}^{\psi}$ from (25)). This RHCP back-lobe level is 17 dB lower than the gain of the main lobe.

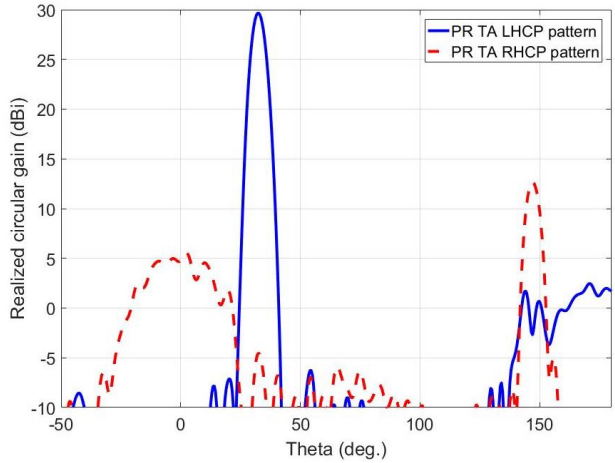

Fig. 11 Simulated performance of phase rotation (PR) TA

V. MEASUREMENT RESULTS

In order to verify the aforementioned comparisons between the two types of cells, the two TAs presented in Fig. 9 were fabricated. For fabrication, each layer of the array was printed on 20 mil Rogers 5880 with 35 μm cladding. Then, the printed layers were aligned and glued together with Rogers 3001 bonding film, which has the same relative permittivity as the Rogers 5880 substrate. The prototypes are displayed in Fig. 12 where the size of the unit-cells and the thickness of the two TAs are compared using the same scale. It is shown that the PR unit-cells are twice of the size of the PD cells while they only have $1/3$ of the PD cells' thickness. The PD-TA weighs about 214 g while the PR-TA weight is less than $1/3$ of this amount and is only 66 g.

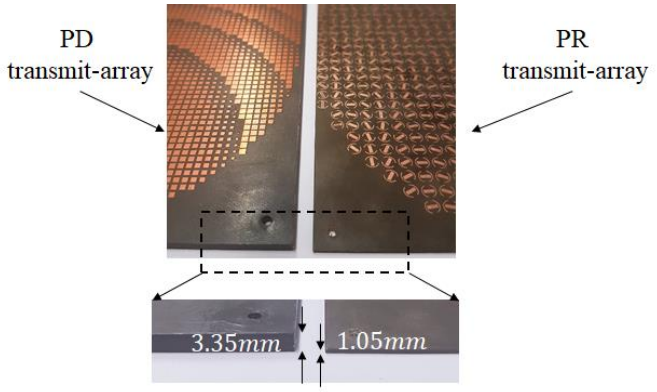

Fig. 12 Prototypes of the PD and PR-TAs. It can be seen that the size of PD cells are half of the size of the PR cells. Also, the PR-TA is much thinner than the PD- TA.

To test both TAs, the standard horn has been replaced by an actual circular polarization feed. The motivation is to compare the PR-TA performance in the same conditions reported for a PD-TA in [16]. Therefore, we use the same type of compact feed system that has been used in [16]. It is a combination of a corner-truncated patch with an intermediate lens to enhance the gain and control the phase center distance. This feed is designed to produce a 12-dBi gain RHCP radiation pattern at 30 GHz. The obtained axial ratio is 2 dB [16] and the 3 dB axial ratio bandwidth is 0.4 GHz.

A 3D printed support was designed to hold the patch antenna, the intermediate lens, and each TA firmly at the precise designed distances from each other, see Fig. 13. The TAs have the same fixed holes' positions so that they can be easily swapped without changing those distances. The setup allows to move the feed continuously along the x-axis from $a = -27$ mm to $a = +30$ mm, with constant F. This leads to a beam scanning interval from 50° and 17°, respectively, according to the calculations presented in [16].

Fig. 14 and Fig. 15 present the measured LHCP and RHCP radiation patterns of the PD- and PR-TA at 30 GHz for various beam tilts between 17° and 50°. The results confirm that the PD-TA preserves the feed polarization, while collimating both the co- and cross polarization components. The scan loss is ≤ 2.8 dB up to 50° tilt angle. The PR-TA converts the feed RHCP to LHCP and presents lower values of the main-beam cross-polarization. The scan loss is ≤ 3 dB for the same range of beam tilts.

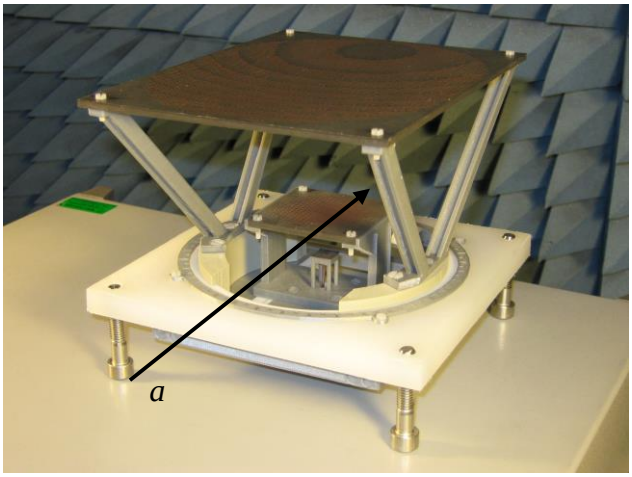

Fig. 13 3D printed setup to hold the TA, the intermediated lens and the patch antenna. The picture shows the PD-TA that can be unscrewed and replaced by the PR-TA. The intermediate lens and the patch can be jointly shifted parallel to the TA, along the a-axis, to steer the main beam in elevation.

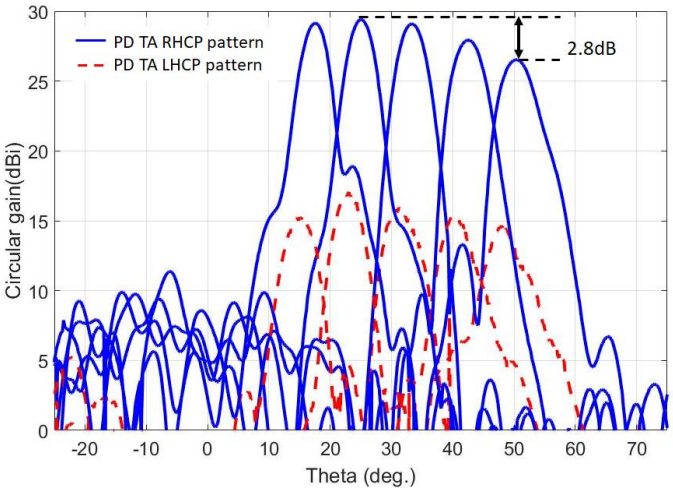

Fig. 14 Measured radiation patterns of PD-TA for beam tilt angles between 17° and 50° at 30GHz, RHCP (solid blue curves) and LHCP (dashed red curves) [16].

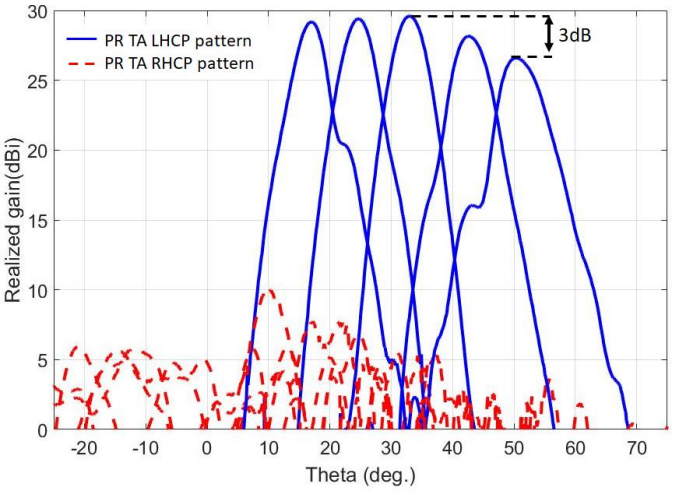

Fig. 15 Measured radiation patterns of PR-TA for beam tilt angles between 17° and 50° at 30GHz, LHCP (solid blue curves) and RHCP (dashed red curves).

Fig. 16 presents the gain versus frequency for each TA when the feed is in the central focal point position of the TAs, corresponding to the main beam direction at $\alpha_0 = 32.5°$. Based

on these results, the 3 dB gain bandwidth of the PD-TA antenna is 2.5 GHz (29 GHz – 31.5 GHz) with 29.1 gain dBi at 30 GHz; whilst the 3 dB gain bandwidth of the PR-TA solution is 1.9 GHz (29 GHz – 30.9 GHz) with 29.5 dBi gain at 30 GHz. The cross-polarization curves of both TAs are presented in the same figure. The cross-polarization level of the PD-TA clearly increases away from the central frequency and this is due to the increasing cross polarization component of the feed. In fact, the patch feed has a narrow circular polarization bandwidth. Since the PD-TA collimates both the co- and cross-polarizations, it inherits the feed poor polarization bandwidth. That is, the reduction in co-polarization gain in the PD-TA is accompanied by an increase in cross-polarization gain. In contrast, the PR-TA filters out the transmitted cross-polarization and collimates only the co-polarization component of the feed radiation pattern making it much lower across the bandwidth. In conclusion, even if the operation bandwidth of the PR cells is narrower than the PD cells (see Fig. 6 and [16], respectively), in the end, both TAs have similar gain bandwidth due to the polarization performance of the feed.

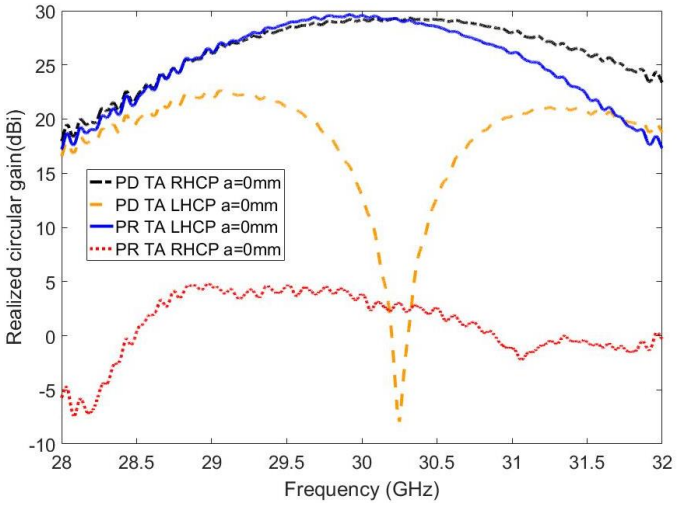

Fig. 16 Realized RHCP gain of the PD-TA (solid black line) and realized LHCP gain of the PR-TA (solid blue line) versus frequency for the feed at the central focal position, that is, when the main beam direction is $\alpha_0 = 32.5°$.

To highlight better the feed cross-polarization filtering effect, Fig. 17 shows the measured axial ratio of both antennas for the main beam direction ($\alpha_0 = 32.5°$), compared to the simulated axial ratio of the isolated feed antenna. It shows that the 3 dB axial ratio bandwidth of the PD-TA is 0.57 GHz (29.98 GHz – 30.55 GHz) which is very similar to the feed bandwidth of 0.4 GHz. In contrast, the main beam axial ratio of the PR-TA antenna is less than 2.3 dB throughout the whole band of 28 GHz – 32 GHz and its value at 30 GHz is only 0.9 dB.

However, as explained in Section II, the PR-TA always directs the cross-polarization component of the feed to $\theta = 0°$ and not to the main beam direction at $\theta = \alpha_0 = 32.5°$. So, it is also important to analyze the cross-polarization level at $\theta = 0°$. It is less than 6.3 dBi within the 28 GHz–32 GHz interval, which is more than 22 dB below the main lobe.

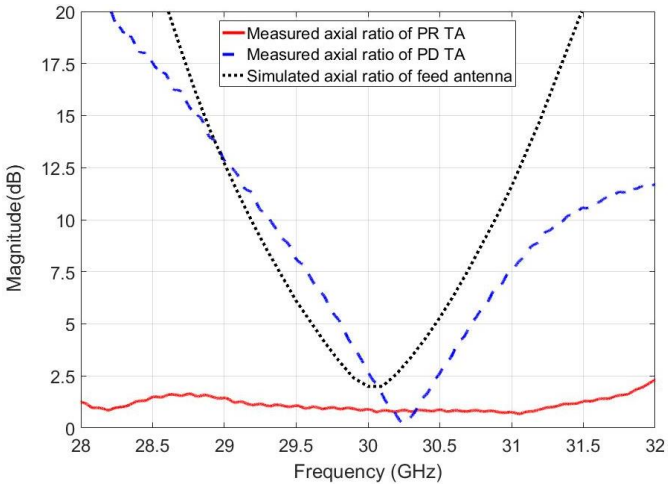

Fig. 17 Simulated axial ratio of the feed antenna vs frequency, compared to the axial ratio of the PR-TA and PD-TA measured for the main beam direction $\alpha_0 = 32.5°$, with the feed at the central focal position.

Finally, it remains to analyze the measured back lobes. Only the extreme positions of the feed provide unperturbed back-lobe measurement, free from the antenna support blocking. We analyze the $a = -27$ mm case, for which the main beam tilts to $\theta = 50°$ and the back lobe to $\theta = 130°$. Fig. 18 superimposes the corresponding circular polarization radiation patterns for the PD-TA and PR-TA. The behavior of the front lobe regarding co- and cross-polarization is similar to what was already discussed for the main beam so we focus only on the back-lobe. The PD-TA collimates both the RHCP and LHCP polarizations toward $\theta = 130°$ at 27.2 dB and 17.4 dB levels below the main lobe, respectively. In contrast, the PR-TA only collimates the RHCP polarization in the back-lobe toward $\theta = 130°$ at 18.9 dB level below the main lobe. Therefore, the PD lens has a higher level of total back lobe at $\theta = 130°$ versus the main lobe, that is -17.6 dB compared to the PR lens that has -18.8 dB.

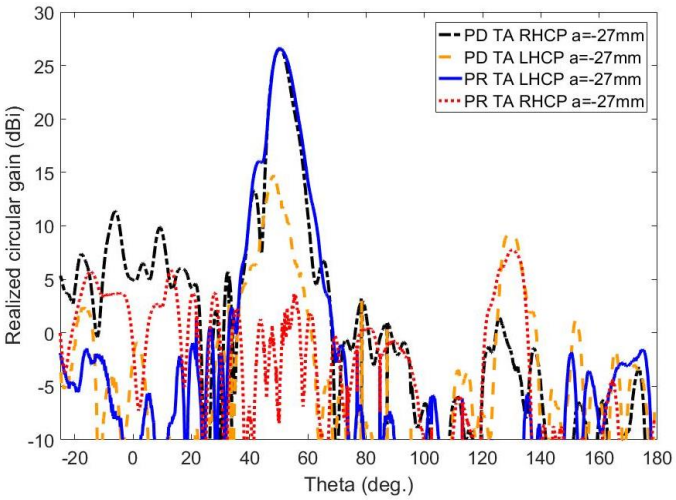

Fig. 18 Measured radiation patterns for PD- and PR-TA with the feed at *a*=-27mm.

VI. Discussion

The above results are summarized in Table II. They do not show drastic differences between the electrical performances of the tested PD- and PR-TAs, safe for the axial ratio, which is significantly better for the latter. On physical aspects, the

thickness and weight are clearly in favor of the PR-TA. However, other intrinsic differences between the two approaches require careful consideration by the designer before choosing one.

TABLE II
PERFORMANCE INDICATORS OF BOTH TRANSMIT-ARRAY TYPES

		PD-TA	PR-TA
Feed 3dB AR bandwidth (GHz)		0.4 (29.85–30.25)	
Area dimensions (mm)		190 × 140	
Thickness (mm)		3.35	1.05
Weight (g)		214	66
Central beam	Gain (dBi)	29.1	29.5
	Axial-ratio (dB)	2.7	0.9
	3dB Gain bandwidth (GHz)	2.5 (29-31.5)	1.9 (29-30.9)
	3dB AR bandwidth (GHz)	0.6 (30–30.6)	>4.0 >(28-32)
	3dB Gain and AR bandwidth (GHz)	0.6	1.9
Scan loss (dB)		2.8	3.0
Back lobe for most titled beam (dB)		-17.6	-18.8

PR-TAs only work optimally for the CP polarization sense for which they are designed. For instance, when designed for an RHCP feed, the PR-TA output beam in transmit mode will be LHCP while the TA will not work with an LHCP feed. In the receive mode, the incoming wave in the above example must be LHCP for the PR-TA to convert and focus it on the feed as a RHCP wave. An incoming RHCP wave will not be focused on the feed. In the general case, an elliptical polarized wave from the feed will be filtered by the PR-TA to transmit only the pure correct sense of CP, which alleviates the requirements for the feed axial ratio. This comes at the cost of losses for the cross CP component, of course. For an LP feed, these losses would amount to 3 dB. So, the axial ratio bandwidth of the PR-TA output beam is not limited by the feed, but only by the cells.

This filtering effect makes PR-TAs unsuitable for applications where polarization diversity and switching between RHCP and LHCP is required, e.g. when moving between adjacent cells in a multi-cell Ka-band satellite services. In addition, it is anticipated that the possibility of designing dual-band PR-TAs with dual-polarization diversity as required for satellite applications is slim.

In contrast, CP PD-TAs preserve the feed's polarization sense, not suffering from the mentioned restrictions. The transmission coefficient bandwidth of PD cells is generally wider than for PR cells, but on the other hand, the best possible axial ratio of the PD-TA is always bounded by the feed axial ratio (see Table II) and can be improved by using a feed with wider axial ratio bandwidth. The feed optimization is out of the paper context. Hence, when analyzing the output beam in terms of the combined bandwidths of gain and axial ratio, as required for satellite communications, the comparison between PD-TA and PR-TA may end up biased by the feed in the PD-TA. In the example of Table II, the PR-TA has triple bandwidth of the PD-TA when considering the combined parameters.

At the design stage, PR cells may be more complex than PD to optimize for bandwidth, given the requirement to provide 180° phase difference between the two-linear polarization responses.

VII. CONCLUSIONS

The paper provides a systematic comparison of phase delay (PD) and phase rotation (PR) cells that are widely used as transmit-array (TA) building blocks, and studies its impact on the performance of circular polarization (CP) TAs. PR cells provide the phase shift through the amount of rotation of its composing elements, which are invariant with rotation. PD cells, instead, provide the phase shift by changing the geometry of its composing elements, thus changing the cell effective permittivity. The choice between these two types of cells for TAs has remained just a matter of opportunity in the literature, the implications on the TA performance never been compared. The paper offers the designer the key information needed to select the preferred option, given the project specifications.

General properties of PD and PR cells, independent of their physical realizations, were derived from basic physical principles. The knowledge of these properties enables anticipating key aspects of the TA performance and decide which type of cells best fit the project requirements. These findings were confirmed using an application example with demanding electrical specifications (high gain, wide-angle beam steering TA at the Ka-band).

The study reveals a couple of unnoticed characteristics of the PR-TA: on one side its wideband cross-polarization filtering characteristic that allows for very good axial ratio output beam. The important consequence of that is that it allows relaxing the feed axial ratio, and it is even possible to use a linear polarization (LP) feed, although with the price of 3 dB loss in this case. On the others side, it is this interesting filtering characteristic of PR-TAs that forbids the switching of the CP sense as required e.g. for satellite communications. In these applications, PD-TAs instead can offer polarization diversity including linear polarization and both senses of CP with similar performance, but limited by the axial ratio bandwidth and magnitude of the feeding antenna.

All the findings were verified and quantified through full-wave simulations and through measurements in the 30 GHz band. Far from being just a TA example, the PR-TA developed for this study is novel and has its own merits compared to the literature in terms of beam scanning range, gain, scan loss, bandwidth and cross-polarization.

VIII. ACKNOWLEDGEMENT

Authors would like to thank the collaboration from C. Brito, J. Frinha, and J. Filicio for prototype construction and A. Almeida for prototype construction and measurements. The authors would also like to thank Rogers Corporation for donating the substrates used for the prototypes.

REFERENCES

[1] S. V. Hum and J. Perruisseau-Carrier, "Reconfigurable reflectarrays and array lenses for dynamic antenna beam control: A review," *IEEE Trans. Antennas Propag.*, vol. 62, no. 1, pp. 183–198, Jan. 2014.

[2] C. A. Fernandes, J. R. Costa, E. B. Lima, and M. G. Silveirinha, "Review of 20 Years of Research on Microwave and Millimeter-wave Lenses at

"Instituto de Telecomunicacoes"," *Antennas and Propagation Magazine, IEEE*, vol. 57, pp. 249-268, 2015.

[3] Y. Zhou, S. Rondineau, D. Popovic, A. Sayeed, and Z. Popovic, "Virtual channel spacetime processing with dual-polarization discrete lens antenna arrays," *IEEE Trans. Antennas Propag.*, vol. 53, no. 8, pp. 2444–2455, Aug. 2005.

[4] R. H. Philion and M. Okoniewski, "Lenses for circular polarization using planar arrays of rotated passive elements*," IEEE Trans. Antennas Propag*., vol. 59, no. 4, pp. 1217-1227, Apr. 2011.

[5] A. Abbaspour-Tamijani, K. Sarabandi, and G. M. Rebeiz, "Antenna-filter-antenna arrays as a class of band-pass frequency-selective surfaces" *IEEE Trans. Antennas Propag.*, vol. 52, no. 8, pp. 1781-1789, Aug. 2004.

[6] D. M. Pozar, "Flat lens antenna concept using aperture coupled microstrip patches," Electron. Lett., vol. 32, no. 23, pp. 2109–2111, 1996

[7] M. A. Al- Joumayly and N. Behdad, "Wideband planar microwave lenses using sub-wavelength spatial phase shifters," *IEEE Trans. Antennas Propag.*, vol. 59, no. 12, pp. 4542-4552, Dec. 2011.

[8] A. K. Iyer and G. V. Eleftheriades, "A multilayer negative-refractive-index transmission-line (NRI-TL) metamaterial free-space lens at X-band," *IEEE Trans. Antennas Propag.*, vol. 55, no. 10, pp. 2746–2753, Oct. 2007.

[9] J. P. Turpin, Q. Wu, D. H. Werner, B. M. Bray, and E. Lier, "Low cost and broadband dual-polarization metamaterial lens for directivity enhancement," *IEEE Trans. Antennas Propag.*, vol. 60, no. 12, pp. 5717–5726, Dec. 2012.

[10] E. Erdil, K. Topalli, N. S. Esmaeilzad, O. Zorlu, H. Kulah, and O. A. Civi, "Reconfigurable nested ring-split ring transmitarray unit cell employing the element rotation method by microfluidics," *IEEE Trans. Antennas Propag.*, vol. 63, no. 3, pp. 1163–1167, Mar. 2015.

[11] L. Di. Palma, A. Clemente, L. Dussopt, R. Sauleau, P. Potier, and P. Pouliguen, "1-bit unit-cell for transmitarray applications in Ka-band," *IEEE Antennas Wireless Propag. Lett*., vol. 15, pp. 560-563, 2016.

[12] C. Chih-Chieh and A. Abbaspour-Tamijani, "Study of 2-bit antenns-filter-antenna elements for reconfigurable millimeter-wave lens arrays," *IEEE Trans. Microw. Theory Techn.*, vol. 54, no. 12, pp. 4498-4506, 2006.

[13] L. Boccia, I. Russo, G. Amendola, and G. Di Masa, "Multi-layer antenna-filter antenna for beam steering transmit-array application," *IEEE Trans. Antennas Propag.*, vol. 60, no. 7, pp. 2287-2300, Jul. 2012.

[14] J. Y. Lau and S. V. Hum, "Reconfigurable transmitarray design approaches for beamforming applications," *IEEE Trans. Antennas Propag.*, vol. 60, no. 12, pp. 5679–5689, Dec. 2012.

[15] Ch. Haung, W. Pan, X. Ma, and X. Luo, "1-bit reconfigurable circularly polarized transmit-array in X-band," *IEEE Antennas and Wireless Propag. Lett.*, vol. 15, pp. 448-451, 2016.

[16] E. B. Lima, S. A. Matos, J. R. Costa, C. A. Fernandes, and N. J. G. Fonseca, "Circular polarization wide-angle beam steering at Ka-band by in-plane translation of a plane lens antenna," *IEEE Trans. Antennas Propag.*, vol. 63, no. 12, pp. 5443-5455, Dec. 2015.

[17] S. A. Matos, E. B. Lima, J. S. Silva, Jorge R. Costa, C.A. Fernandes, N. J. G. Fonseca, J. R. Mosig, "High gain dual-band beam steering transmitarray for satcom terminals at Ka band," *IEEE Trans. Antennas Propag.*, vol. 65, no. 7, pp. 3528 - 3539, Jul. 2017.

[18] N. Cagnon and A. Petosa, "Using rotatable planar phase shifting surfaces to steer a high-gain beam," *IEEE Trans. Antennas Propag.*, vol. 61, no. 6, pp. 3086-3092, Jun. 2013.

[19] M. Tripodi, F. Dimarca, T. Cadili, C. Mollura, F. DiMaggio, and M. Russo, "Ka band active phased array antenna system for satellite communication on the move terminal," European Conference on Antennas and Propagation (EuCAP), Rome, Italy, Apr. 2012.

[20] L. Di Plama, A. Clemente, L. Dssopt, R. Sauleau, P. Potier, and P. Pouliguen, "Circularly-polarized reconfigurable transmitarray in Ka-band with beam scanning and polarization switching capabilities," *IEEE Trans. Antennas Propag.*, vol. 65, no. 2, pp. 529-540, Feb. 2017.

[21] S. Gao, Q. Luo, and F. Zhu, "Introduction to circularly polarized antennas," in Circularly Polarized Antennas, Ed. UK: Wiley, 2014, pp. 1-25.

[22] L. D. Plama, A. Clemente, L. Dussopt, R. Sauleau, P. Potier, and Ph. Pouliguen, "Circularly polarized transmit-array with sequential rotation in Ka-band," *IEEE Trans. Antennas Propag.*, vol. 63, no. 11, pp. 5118-5124, Nov. 2015.

[23] P. Naseri, F. Khosravi, and P. Mousavi, "Antenna-filter-antenna-based transmit-array for circular polarization application," *IEEE Antennas Wireless* Propag. Lett., vol. 16, pp. 1389 - 1392, 2017.

[24] ANSYS® High Frequency Electromagnetic Field Simulation, Release 18.0: http://www.ansys.com.

[25] E. B. Lima, S. Matos, J. Costa, and C. A. Fernandes, "Evaluation of the phase discretization effect in transmitarrays formed by sub-wavelength patches," European Conf. on Antennas & Propagation (EuCAP), Lisbon, Portugal, April 2015.

[26] P. Naseri, R. Mirzavand, and P. Mousavi, "Dual-band circularly polarized transmit-array unit-cell at X and K bands," in Proc. 10th Eur. Conf. Antennas Propag. (EuCAP), Davos, Switzerland, Apr. 2016, pp. 1–4.

Parinaz Naseri (S'14) received the B.Sc. degree in Electrical Engineering (Telecommunications) from the University of Tehran, Tehran, Iran, in 2013 and received M.Sc. degree in Electrical Engineering from the University of Alberta, Edmonton, Canada in 2017. She joined Instituto de Telecomunicações as a grant researcher in September 2016. Her present research interests include frequency selective surfaces, transmit-arrays, reflect-arrays, mm-wave antenna designs.

Sérgio A. Matos (S'05–M'16) received the Licenciado, M.Sc., and Ph.D. degrees in electrical and computer engineering from Instituto Superior Técnico (IST), University of Lisbon, Lisbon, Portugal, in 2004, 2005, and 2010, respectively.

He is currently a Researcher with the Instituto de Telecomunicações (IT), Lisbon, Portugal. He is also an Assistant Professor at the Departamento de Ciências e Tecnologias da Informação, Instituto Universitário de Lisboa (ISCTE-IUL). He is the co-author of 60 technical papers in international journals and conference proceedings. His present research interests include electromagnetic wave propagation in metamaterials, flat-lens design and transmit arrays.

Jorge R. Costa (S'97–M'03–SM'09) was born in Lisbon, Portugal, in 1974. He received the Licenciado and Ph.D. degrees in electrical and computer engineering from the Instituto Superior Técnico (IST), Technical University of Lisbon, Lisbon, Portugal, in 1997 and 2002, respectively.

He is currently a Researcher at the Instituto de Telecomunicações, Lisbon, Portugal. He is also an Associate Professor at the Departamento de Ciências e Tecnologias da Informação, Instituto Universitário de Lisboa (ISCTE-IUL). His present research interests include lenses, reconfigurable antennas, MEMS switches, UWB, MIMO and RFID antennas. He is the coauthor of four patent applications and more than 150 contributions to peer reviewed journals and international conference proceedings. More than thirty of these papers have appeared in IEEE Journals. Prof. Costa served as an Associate Editor for the IEEE Transactions on Antennas and Propagation from 2010 to 2016 and he was a Guest Editor of the Special Issue on "Antennas and Propagation at mm- and Sub mm-Waves", from the IEEE Transactions on Antennas and Propagation, April 2013. He was the Co-Chair of the Technical Program Committee of the European Conference on Antennas and Propagation (EuCAP 2015) in Lisbon and General Vice-Chair of EuCAP 2017 in Paris.

Carlos A. Fernandes (S'86–M'89–SM'08) received the Licenciado, MSc, and PhD degrees in Electrical and Computer Engineering from Instituto Superior Técnico (IST), Technical University of Lisbon, Lisbon, Portugal, in 1980, 1985, and 1990, respectively. He joined IST in 1980, where he is presently Full Professor at the Department of Electrical and Computer Engineering in the areas of microwaves, radio wave propagation and antennas. He is a senior researcher at the Instituto de Telecomunicações and member of the Board of Directors. He has co-authored a book, 2 book chapter, more than 180 technical papers in peer reviewed international journals and conference proceedings and 7 patents in the areas of antennas and radiowave propagation modeling. His current research interests include dielectric antennas for millimeter wave applications, antennas and propagation modeling for personal communication systems, RFID and UWB antennas, artificial dielectrics and metamaterials. He was a Guest Editor of the Special Issue on "Antennas and Propagation at mm- and Sub mm-Waves", from the IEEE Transactions on Antennas and Propagation, April 2013.